Smart Structures and Systems, Vol. 5, No. 4 (2009) 397-413
DOI: http://dx.doi.org/10.12989/sss.2009.5.4.397

Diagnostic/prognostic health monitoring system and evaluation of a composite bridge

A. Mosallam* and R. Miraj

University of California, Civil and Environmental Engineering Department, Irvine, CA 92697, U.S.A.

F. Abdi

AlphaSTAR Corporation, Long Beach, CA 90804, U.S.A.

(Received October 3, 2008, Accepted November 1, 2008)

Abstract. Composite bridges offer many advantages compared to current steel and aluminum bridges. This paper presents the results of a comprehensive on-going research program to develop innovative Diagnostic Prognostic System (DPS) and a structural evaluation of Composite Army Bridge (CAB) system. The DPS is founded on three technologies: optical fiber sensing, remote data transmission, and virtual testing. In developing this system, both laboratory and virtual test were used in different damage scenarios. Health monitoring with DPS entailed comparing live strain data to archived strained data in various bridge locations. For field repairs, a family of composite chords was subjected to simple ramp loads in search of ultimate strength. As such, composite bridge specimens showcased their strengths, heralded the viability of virtual testing, highlighted the efficacy of field repair, and confirmed the merits of health monitoring.

Keywords: health monitoring; fiber optical sensors; progressive failure analysis; composite bridge; diagnostic prognostic system; repair.

1. Introduction

In recent years, the use of advanced composites to build bridges has become an attractive topic of research for many structural engineers (Mosallam, *et al*. 2003, Abdi, *et al*. 2003). Composite bridges provide numerous attractive features. The lightweight characteristic of composites is essential to achieve the goal of rapid operational mobility. However a fatigue-cycled bridge may have damages that are due to punctures, impact loads and deployment issues related to handling, dropping or dragging (Abdi, *et al*. 2003).

Internal damage in composites is often initiated as matrix cracking due to tensile stresses transverse to fiber orientation. Nevertheless, damage initiation and progression characteristics for composite structures are diverse. In the presence of stress concentrations, or defects, initial damage may also include fiber fracture. Due to the many possibilities with material combinations, composite geometry, fiber orientations, and loading conditions, it is essential to have an effective computational capability to predict the behavior of composite structures for any loading, geometry, composite material combinations, and

*Corresponding Author, E-mail: mosallam@uci.edu

boundary conditions.

The predictions of damage initiation, growth, accumulation, and propagation to fracture are important to evaluate the load carrying capacity of composite structures. Quantification of the structural fracture resistance is also required to evaluate the durability/life of composite structures. A computational simulation method has been developed for this purpose. The method is able to simulate damage initiation, damage growth, and fracture in composites under various loading, considering also the effects of residual stresses and environmental conditions (Chamis 1969). The objective of the paper is to integrate this simulation capability into health monitoring. The first part of this study examines the processes and components used to generate the DPS that was proposed and designed by the first author. In the second component, DPS is used to monitor the health of a composite beam. In the final part of this study, undamaged, damaged and repaired composite chords are subjected to simple ramp loads in search of ultimate strength. The resulting values of strength serve to gauge the efficacy of the repair methodology and provide the foundation for real world applications.

2. Methodology

2.1. Progressive fatigue failure analysis

The simulation analysis for durability, reliability, and risk assessment is based on an enhanced software system technology, the General Optimizer Analyzer (GENOA), which takes a full-scale finite element model and breaks the material properties down to the microscopic level, where material properties are updated for each iteration, reflecting any changes resulting from damage or crack propagation. The hierarchical approach implemented in GENOA allows integration of a wide range of specialized programs, from micro to macro, into an existing verified progressive failure and probabilistic analysis tool. This makes it possible to accurately evaluate the behavior Polymer Matrix Composites (PMC) structures, such as Fig. 1, by way of progressive failure analysis and virtual testing, which is based on the physics and micro/macro mechanics of materials, manufacturing processes, available data, and service environments. This approach takes progressive damage and fracture processes into account and accurately assesses reliability by predicting failure initiation and progression based on constituent material properties. The life prediction codes utilize and integrate: 1) finite element structural analysis, 2) micro-mechanics, and fracture mechanics options, 3) damage progression tracking, 4) probabilistic risk assessment, 5) minimum damage design optimization, and 6) material characterization codes to scale up the effects of local damage mechanisms to the structure level to evaluate overall performance and integrity. A significant advantage of using a life prediction tool in the

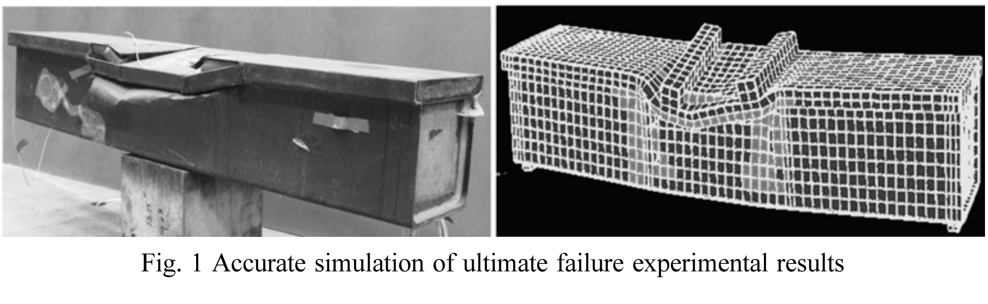

Fig. 1 Accurate simulation of ultimate failure experimental results

design process is that the number of experimental tests at the component and substructure levels can be substantially reduced. The damage progression module relies on a composite mechanics code (Murthy and Chamis 1986) for composite micromechanics, macro-mechanics, laminate analysis, as well as cyclic loading durability analysis, and calls a finite element analysis module that uses anisotropic thick shell elements to model laminated composites (Nakazawa, *et al.* 1987).

Imposing failure criteria locally within each micromechanics sub-volume carries out progressive damage and fracture simulations. Micromechanics sub-volumes are obtained by subdividing each micromechanics volume into regions with characteristic fiber configuration. Within each sub-volume, local coordinate orientation in the material coordinate systems is identified. At each individual load step, the stresses and strains obtained through 3D woven composite micro stress analysis are checked according to distinct failure criteria. The first twelve failure modes are associated with the positive and negative limits of the six local stress components in the material direction as follows:

$$S_{l11C} < \sigma_{l11} < S_{l11T}, \tag{1a}$$

where S_{l11C} is longitudinal compressive strength and S_{l11T} is longitudinal tensile strength

$$S_{l22C} < \sigma_{l22} < S_{l22T}, \tag{1b}$$

where S_{l22C} is transverse compressive strength and S_{l22T} is transverse tensile strength

$$S_{l33C} < \sigma_{l33} < S_{l33T}, \tag{1c}$$

where S_{l33C} is normal compressive strength and S_{l33T} is normal tensile strength

$$S_{l12(-)} < \sigma_{l12} < S_{l12(+)}, \tag{1d}$$

where $S_{l12(-)}$ is in-plane negative shear strength and $S_{l12(+)}$ is in-plane positive shear strength

$$S_{l23(-)} < \sigma_{l23} < S_{l23(+)}, \tag{1e}$$

where $S_{l23(-)}$ is transverse-normal negative shear strength, $S_{l23(+)}$ is transverse-normal positive shear strength

$$S_{l13(-)} < \sigma_{l13} < S_{l13(+)}, \qquad 1(f)$$

where $S_{l13(-)}$ is longitudinal-normal negative shear strength and $S_{l13(+)}$ is longitudinal-normal shear strength

The thirteenth failure mode is a combined stress failure criterion, or modified distortion energy (MDE) failure criterion that is obtained by modifying the usual distortion energy failure criterion. The modification takes into account the significant differences in the stress limits of the longitudinal and transverse directions of an orthotropic composite ply. Each component of ply stress is normalized with respect to its limiting strength. The MDE failure criterion has been demonstrated to be a good predictor of combined stress failure in composites. It may be considered as a variation of the Tsai-Hill theory (Tsai 1968, Hill 1950). The MDE failure criterion (Chamis 1969) can be expressed as:

$$\left(\frac{\sigma_{l11\alpha}}{S_{l11\alpha}}\right)^2 + \left(\frac{\sigma_{l22\beta}}{S_{l22\beta}}\right)^2 - K_{l12\alpha\beta}\frac{\sigma_{l11\alpha}\sigma_{l22\beta}}{S_{l11\alpha}S_{l22\beta}} + \left(\frac{\sigma_{l12S}}{S_{l12S}}\right)^2 < 1 \tag{2}$$

Here α and β indicate tensile or compressive stresses, $S_{l11\alpha}$ is the local longitudinal strength in tension or compression, $S_{l22\beta}$ is the transverse strength in tension or compression, and the directional interaction factor is defined as:

$$K_{l12\alpha\beta} = K'_{l12\alpha\beta}\frac{(1 + 4\nu_{12} - \nu_{13})E_{12} + (1 - \nu_{23})E_{11}}{[E_{11}E_{22}(2 + \nu_{12} + \nu_{13})(2 + \nu_{21} + \nu_{23})]^{1/2}} \tag{3}$$

Here $K'_{l12\alpha\beta}$ is a theory-experiment correlation factor. The directional interaction factor reduces to unity for homogeneous isotropic materials.

2.2. DPS background

The health monitoring of civil engineering infrastructure has grown rapidly over the last decade. While most systems have sought to provide information as to the state or health of a structure, few have attempted to prognosticate events and estimate residual capacity. The DPS, developed to address this shortfall, was created as part of program that sought innovative approaches and techniques to repair composite bridges in the field. Specifically, DPS provides a mechanism to remotely capture strain data from a structure in response to a live loading event. Next, DPS remotely transmits the data from the structure to a web server hosting the Collaborative Virtual Testing (CVT) software. The central data server not only supports GENOA analysis but also maintains a vast arsenal of archived simulations, including multiple progressive failure models of the composite bridge in question and specific information on maximum threshold strains unique to the that structure. Thirdly, a CVT operator may compare live strain data transmitted from the field to simulated maximum threshold strains and, as such, identify areas of damage or failure. Here, it should be noted that CVT supports many GENOA features, which allow a pro-active operator to extract vast amounts of information and draw numerous conclusions from simulation models, related to the remote structure, that have experienced damage. In all there are nine steps associated with DPS, as identified in Fig. 2, with the final features providing insight into residual strength as a result of repair. DPS combines real-time remote sensing with the power of virtual testing and progressive failure analysis. DPS not only identifies damage but also determines residual properties and finds the best possible repair solution from a mix of available materials.

DPS is dependent upon four core technologies. These technologies include virtual testing and progressive failure analysis; event driven data interrogation; Internet data transmission; and data processing and data storage through Collaborative Virtual Testing (CVT).

2.3. Virtual testing

Virtual testing and GENOA lie at the heart of DPS. Together, they provide an ability to evaluate component behavior, identify maximum strain thresholds and predict failure. GENOA integrates nonlinear finite element structural analysis; composite micro-mechanics; and fracture mechanics to scale up the effects of local damage mechanisms to the structure level and evaluate overall performance and integrity. Virtual testing with GENOA uses material test data and uncertainty at the micro level to simulate structural level damage initiation, growth, and propagation processes. In this manner, changes in structural load paths with damage progression are accurately identified based on physics and material properties. With GENOA, DPS may confidently compare live data from a composite bridge to simulated data generated by an accurate finite element model that replicates the composite bridge and all applicable loads.

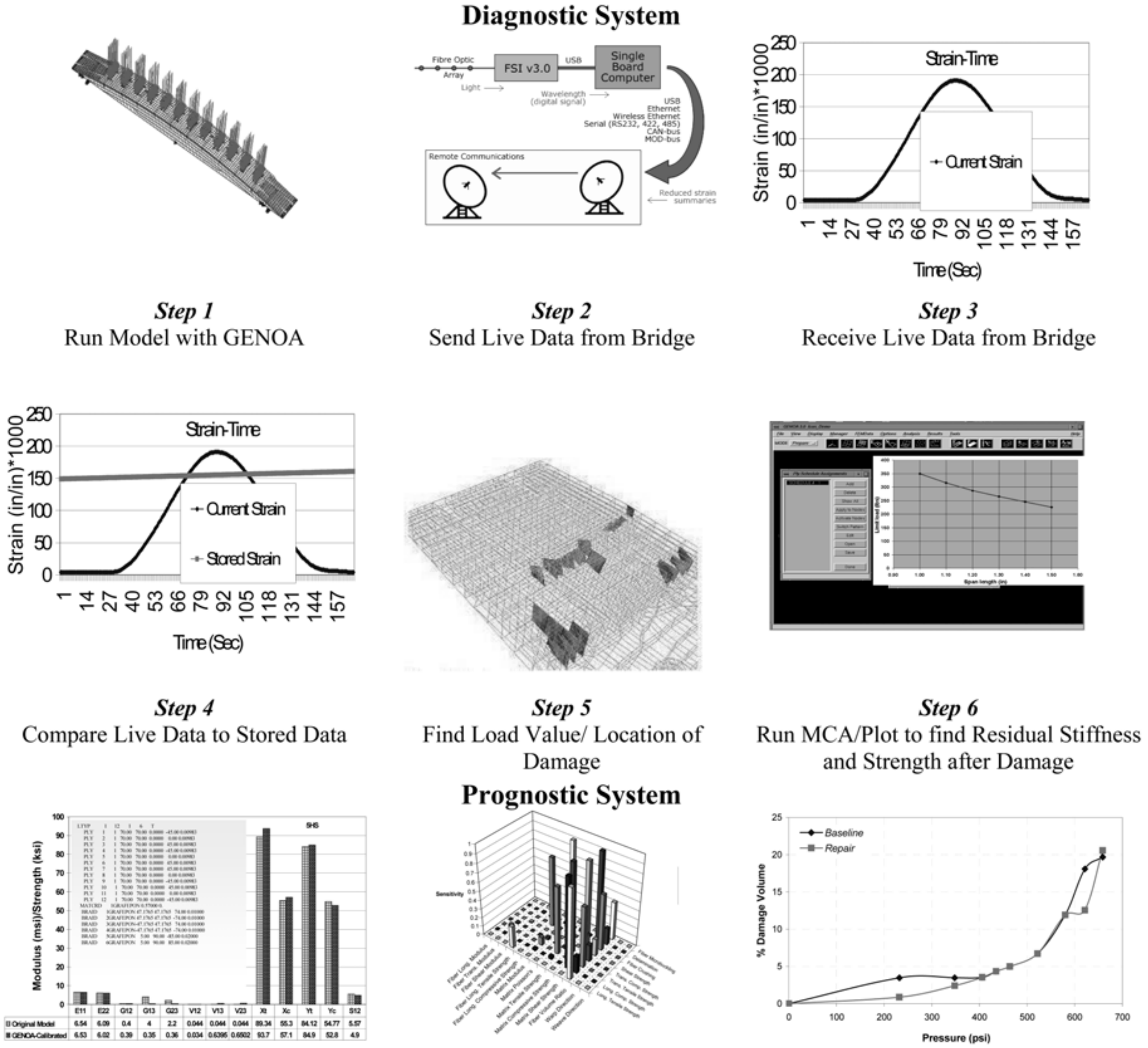

Step 1
Run Model with GENOA

Step 2
Send Live Data from Bridge

Step 3
Receive Live Data from Bridge

Step 4
Compare Live Data to Stored Data

Step 5
Find Load Value/ Location of Damage

Step 6
Run MCA/Plot to find Residual Stiffness and Strength after Damage

Step 7
*List Available Repair Material in Databank

Step 8
Run MUA/Find Failure Sensitivity to Material and % constituents; identify best recipe for repair

Step 9
Evaluate/Compare Performance of repair

Fig. 2 Nine step DPS methodology

2.4. Embedded sensors and optical fiber interrogation

The Fiber Bragg Grating (FBG) sensor has become the most commonly adopted form of fiber optic sensing due to its small size. When coupled with a standard interrogation unit up to one hundred sensors may be employed within a single strand, which in turn would be either embedded within the bridge during fabrication or mounted on the surface. If the fiber sensor is strained or pulled from each end of the FBG, planes within the sensor will shift apart and the wavelength that gets reflected will increase. By knowing the unstrained FBG wavelength, one can directly calculate the strain on the fiber at the point where the FBG resides from the wavelength shift of the reflected light. The strain at many points within a fiber can be obtained by monitoring the wavelength of multiple sensing elements dispersed along the fiber.

The DPS Fiber Sensor Interrogator (FSI) system is used for reading real-time strain and temperature data from an array of multiple FBG sensors along a single channel. When ready to extract data, the FSI transmits a broad band light pulse into the fiber in order to illuminate the FBG sensor array. Next, it provides amplification and time-based gating of the reflected sensor signals and examines each sensor's peak reflected wavelength to measure strain. Finally, each sensor peak wavelength is ported to a secondary communication device for delivery to the outside world.

2.5. Data transmission

Reliable data communication is essential for the success of the DPS. For that reason, redundancy and robustness are key criteria for the final system. Currently, as shown in Fig. 3, DPS utilizes a cellular communications network with a web server to route data from the FSI through an Internet Service Provider (ISP) and on to CVT. Additional protocols are in place and under development. These include an existing communications system that utilizes traditional cellular telephone pc-card technology to allow modem-to-modem communication over a standard cellular telephone network and a proposed commercial satellite communication system that will utilize off-the-shelf hardware to communicate directly with the CVT while employing sophisticated data compression and encryption routines coupled with scheduled or event-driven data deliveries to reduce the shear volume of data and lower the overall cost of transmission.

2.6. Collaborative Virtual Testing, central data hub

Collaborative Virtual Testing (CVT) software was developed to facilitate cooperation among geographically dispersed team members. As such, CVT capabilities include conducting secure net meetings; uploading test data; storing presentations, reports, and publications; generating simulation input; running advanced engineering simulations; viewing simulation results; and sorting and searching historical simulation within the archive. More to the point, CVT was designed to allow widely distributed users to run

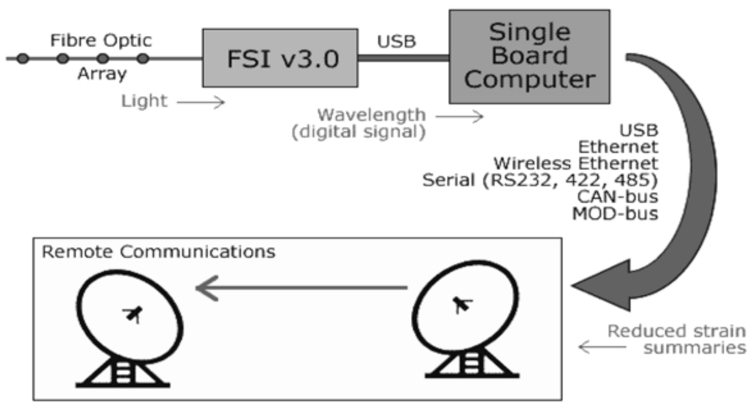

Fig. 3 The DPS remote communications system architecture

GENOA models on the Internet and share access to results. Access to CVT is controlled by private user accounts with tight security features. Administrator defined user privileges dictate the extent to which a given user may have access to archived simulations. When combined with DPS, CVT becomes a central data hub, accessible to anyone with appropriate credentials, where live data from the field is compared in real time to simulated strain values associated with archived modules. More importantly, CVT provides DPS with a suite of intelligent tools and custom interactive software to compare data sets, recognize damage, identify the mechanisms that precipitated damage, determine post-damage residual stiffness and strength, recognize material sensitivities and propose logical repair solutions.

2.7. Proposed areas of growth

DPS has been designed to exploit the best features of its core technologies and deliver an interactive tool that can be used on-site or in the laboratory. Yet, new capabilities and modifications are being examined all the time. In the future, data delivery from the remote location may include displacement, rotation, environmental conditions, type of damage, location of damage, degree of damage, and intelligent vehicle identification that occurs either before or during a bridge crossing. Finally, in its current configuration, data is pushed from the remote structure to the CVT evaluation center. Because of the inherent restrictions of satellite technology, engineers at the CVT will be given the ability to pull data from the interrogation unit on demand or identify a schedule for data delivery where load/strain events are captured, encrypted, compressed and stored locally before being delivered on a hourly, daily, weekly or monthly basis. As such, with regard to power consumption, the interrogation box may automatically move to sleep mode until awakened at an appropriate time for a load event.

3. Numerical modeling & experimental verifications

3.1. DPS component configuration and validation

In this program, several test articles were used in the development of DPS. Large specimens were evaluated, including the full-scale CAB that was tested at the University of California at San Diego (UCSD) and a scaled-down mockup of the Modular Composite Bridge (MCB) that was tested at the University of California at Irvine (UCI) Structural Engineering Testing Hall (SETH). Additional components consisted of sections that were cut from the MCB prototype with the objective of using those sections to develop and demonstrate the field repair process.

Mockup test specimens were fabricated and instrumented with Fiber Bragg Grated (FBG) optical sensors and later tested at UCI. Between 4 and 8 sensors were installed on each test article. In all cases, the sensors were used to provide verification data for the simulated progressive damage models that were undertaken with the General Optimal Analyzer (GENOA) code developed by Alpha Star Corporation (ASC) and utilized by UCI.

During fabrication, UCI and ASC personnel evaluated the reliability of the installed optical fiber interrogation system. Testing was carried out using an FSI V3 serial 030054 interrogation box and a Dell Latitude laptop. Connection was via USB link and standard Lab VIEW® interrogation software. Later, the completed interrogation system was coupled with live tests and simulations models to provide the backbone of DPS and system prognostication.

3.2. MCB composite materials

Prior to undertaking detailed simulation studies of the MCB and the mockup beams, UCI and ASC personnel completed a detailed verification of GENOA's ability to estimate the material properties of the constituent materials used to fabricate the test articles. The composite material properties were calibrated by using GENOA Material Constituent Analyzer (MCA) & Progressive Failure Analysis (PFA) Codes. A total of four different composite materials, comprising the CAB structure, were calibrated based the coupon level experiments. Prior to performing the calibration process, original mechanical information, in the form of test data, was identified from Abdi, *et al*. (2003). The results of the calibration process identified several variations, especially in the shear modulus strength and Poisson's ratios. As expected, the experimental and the calibrated results for unidirectional laminates agreed well. Table 1 shows the results obtained from the calibration analysis for different constituent materials.

3.3. CAB progressive failure simulation under static cyclic and fatigue

The next GENOA simulation involved cyclic tests of a "single-treadway" of the CAB. Once verified, the simulation was extended to check fatigue life of CAB and prognosticate on its long-term behavior. A progressive failure analysis model under low cycle fatigue loading was used to evaluate the performance of the CAB subjected to "moving" loads. The model was constructed for a single treadway with the maximum bending load pattern.

The cyclic test loading sequence was converted to load spectrum by using the rainflow count as defined in ASTM E1049-85. Since the loading sequence does not have constant loading amplitude, fatigue strength based on traditional S-N curves cannot be used directly to degrade material properties. Accordingly, the linear cumulative damage rule, i.e. Miner's rule, was used to predict damage under loading. Miner's rule assumes that the total life of a part can be estimated by adding up the percentage of the life consumed by each stress cycle. Where n_1, n_2,..., n_k represent the number of cycles of operation at

Table 1 Calibrated and original mechanical properties of laminates

Modulus (GPa) / Strength (MPa)	5HS		Triaxial		Unidirectional		Biaxial	
	Experimental	GENOA-Calibrated	Experimental	GENOA-Calibrated	Experimental	GENOA-Calibrated	Experimental	GENOA-Calibrated
E11	6.54	6.53	5.10	5.28	11.85	11.95	1.73	1.79
E22	6.09	6.02	1.89	2	0.63	0.63	1.73	1.79
G12	0.4	0.39	2.23	2.2	0.36	0.367	4.337	4.38
G13	4	0.35	0.68	0.39	0.23	0.367	4.337	0.49
G23	2.2	0.36	0.68	0.36	0.23	0.24	0.627	0.49
V12	0.044	0.034	0.13	0.76	0.325	0.323	0.81	0.82
V13	0.044	0.6395	0.84	0.20	0.325	0.3235	0.81	0.1163
V23	0.044	0.6502	0.84	0.44	0.325	0.5073	0.81	0.1163
Xt	89.34	93.7	82.92	57.9	128	127.8	23.2	23.4
Xc	55.3	57.1	48.26	35.6	77.84	77.48	28.6	24
Yt	84.12	84.9	16.64	12.6	2.41	2.59	23.2	23.4
Yc	54.77	52.8	19.29	18.4	11.49	12.3	28.6	24
S12	5.57	4.9	18.93	25.2	4.73	4.9	10.04	46.86

specific stress levels and $N_1, N_2, \ldots, N_k$ represent the life (in cycles) at these same stress levels, then

$$\frac{n_1}{N_1} + \frac{n_2}{N_2} + \ldots + \frac{n_k}{N_k} = 1 \quad \text{or} \quad \sum_{j=1}^{k} \frac{n_i}{N_i} = 1 \tag{4}$$

However, variable amplitude fatigue failure of fiber-reinforced composites is very complex and requires a fundamental understanding of applicable failure mechanisms. While many experimental investigations on fatigue of composites have been performed at constant amplitude, the mechanical load-time history acting on a composites component in service is normally of variable amplitude. Unfortunately, variable amplitude fatigue loading does not always agree with linear cumulative damage rules. Fortunately, nonlinear models have been developed to expand the linear cumulative damage rule and include the effects of load sequence and loading level on the fatigue life prediction. Marco-Starkey suggests that cumulative damage may be represented by simple nonlinear formula. GENOA provides an option of using the thermodynamic cumulative damage constitutive law derived by Lee at Delphi Research Lab for a multi-stage fatigue load sequence, where 0.1 degradation factors were converted to a S-N curve for each material.

The single treadway GENOA model consists of 9,124 nodes and 14,514 elements. Of these, 9,911 laminate elements model the *sidewalls, tension rail, deck skins, and bulkheads*; 692 plate elements model the launch rail and end caps; 3,814 solid elements model the balsa wood core; and 88 beam elements model the sidewall stiffeners. The elements are defined using 62 material property sets that account for different materials and specific layups used in the bridge, including local ply drop-offs in the tension rail and local build-up of the sidewalls.

Using GENOA, a Progressive Failure Fatigue Analysis (PFFA) was performed on the CAB subjected to simulated cyclic loads. The UCSD experimental program was performed from cycles 1 through 1,001 as shown in Table 2. Throughout the cyclic test, there were no indications of treadway damage or stiffness or strength degradations. All strain gages and pots behaved linearly with no hysteresis. The test showed little change in strains and displacements during the 1,000 cycles.

The simulation showed the same trend as that observed during the actual test. Results indicated that before cycle 16,380, there was a slight change in the mid-span displacement. However, after cycle 16,380, the mid-span deflection changed dramatically, and the ultimate failure occurred at the cycle 475,140.

Fig. 4 shows damage initiation and propagation in both the single and double treadway designs. With regard to the single treadway, one can see that damage initiate at the tension rail at cycle 32,768, then propagate along the rail by removing the elements. After cycle 131,070, the structure fails due to the fracture, and tension rail damage is due to longitudinal tension failure. Collectively, the results suggest that GENOA can accurately mimic test results and, given appropriate inputs, potentially predict behavior. This capability, when coupled with real-time interrogation of an article or specimen, will make DPS a formidable tool.

Table 2 Cyclic strains & displacements in lower tension rail

Cycle	Strain (10^{-6} mm/mm)	Displacement (mm)
1	1689.5	-36.42
101	1668.2	-36.88
601	1672.7	-37.34
1001	1648.0	-38.07

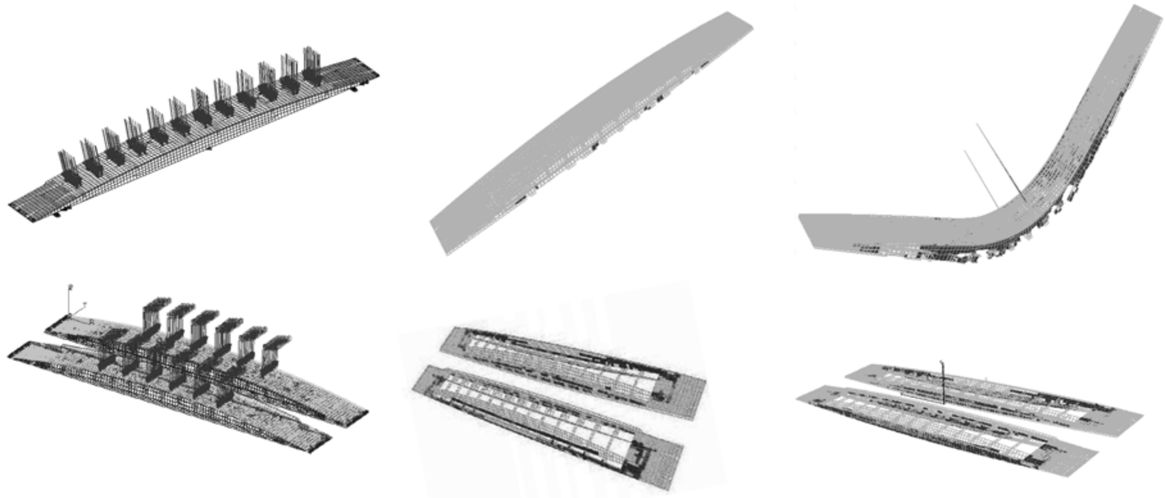

Fig. 4 Progression of damage on one and two-treadway CAB model

3.4. PFA of the two-treadway CAB model

The two-treadway GENOA model was developed from actual Military Load Class (MLC) data. In this model, the maximum curb step is 3.94 in (100 mm); the end-ramp slope is 1:5; the treadway width is 61.0 in (1.55 m); the overall width is 157.4 in (4.00 m); and the overall height is less than 157.4 in (4.0 m). The overall length of the specimen and the model was 551.0 in (14 m). The model consists of 18,426 nodes and 29,027 elements. The elements are defined using 62 material property sets to account for the different materials and lay-ups in the bridge, including the local ply drop-offs in the tension rail and local build-up of the sidewalls near the end-ramps.

A Progressive Failure Analysis (PFA) was performed on the model of two-treadway CAB under the design load for MLC-100 vehicle. The final failure for this case occurred at total load of 511 kips (2268.8 kN) or a pressure load of 464 psi (3.25 MPa) on each patch. Damage energy release rate history as a function of fatigue cycle and load level was also examined. Here, percent damage volume increase reveals the limit load capability. In this case, the limit state is predicted to be the initial load condition. In the Damage Energy Release Rate (DERR), the stick and slip points identify the load at which successive internal damage is occurring. Once again, the results corresponded to the limited data set associated with actual testing and confirmed the viability of this process as a critical component of DPS.

3.5. Virtual testing of CAB after fire exposure

The following sections present the results of the GENOA simulation to predict the post-fire residual strength of the CAB Bridge. This simulation followed a three-pronged methodology. In the first step, the deck of CAB was subjected to a thermal load, simulating fire, and thermal analysis with MSC. NASTRAN was used to obtain the resulting temperature distribution across the deck. Next, the model was converted to a GENOA format, the temperature distribution was used as an input thermal load, and a progressive failure analysis was employed to evaluate the damage distribution and damage pattern due to fire exposure. Here, the progressive failure analysis used a multi-factor interaction model to

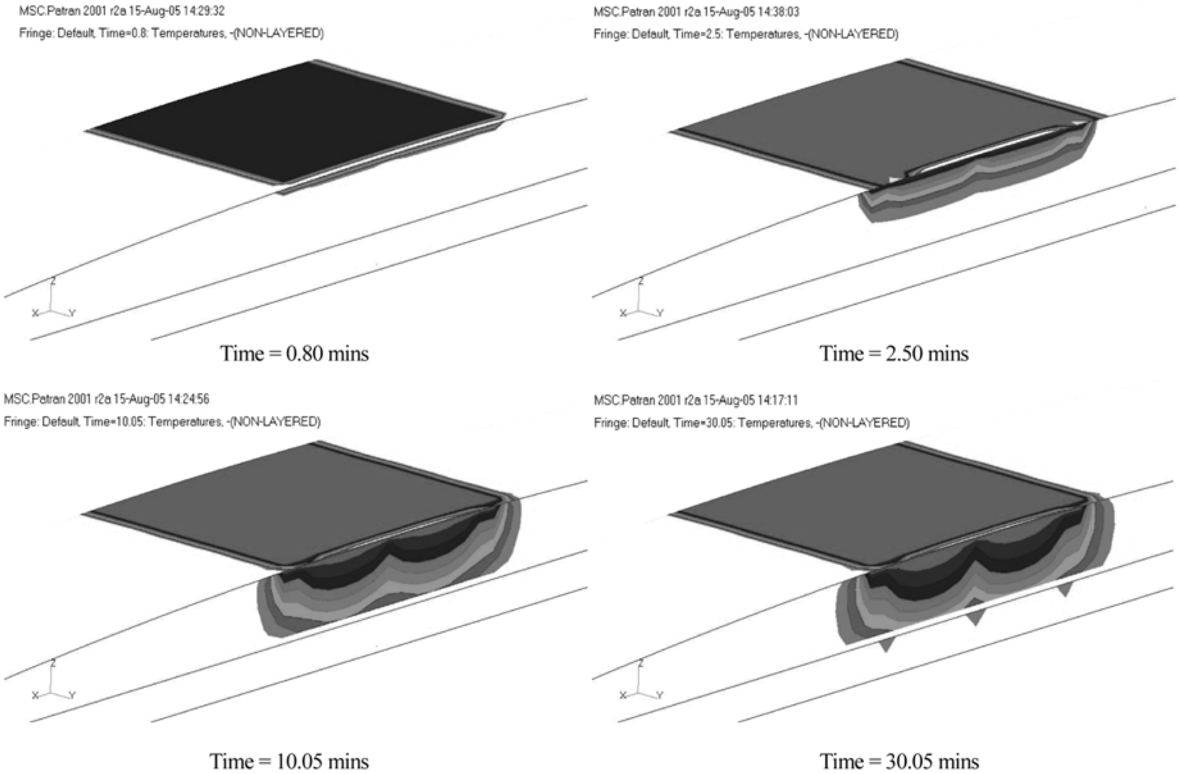

Fig. 5 Temperature distribution at different time intervals: Blue-2000°F and Yellow-70°F

assess composite material degradation with respect to temperature. Finally, a damage index, which records the damage distribution and damage pattern, was imported, along with the selected load case, into the GENOA progressive failure analyzer in order to find a final post-fire residual strength of CAB, which corresponds to the ultimate load of the degraded member subject to the load case.

For this study, the Max Shear loading was selected as the reference load case. As a first step, the deck of CAB was subjected to a thermal load on its center top. The fire reached a temperature of 2,000°F, which resulted in an incident head flux of 200 kW/m^2. This extreme temperature was achieved after a period of 1 minute and remained in effect for the duration of the fire. A radiation boundary condition was applied to all of the outer surfaces and MSC.NASTRAN was used to obtain the corresponding temperature distribution. Fig. 5 shows the temperature distribution at various times. The heat propagates through balsa layers towards the bottom of CAB and temperature distribution enters steady situation after 40 minutes.

Next, the steady state temperature distribution from thermal analysis is used as a load for the GENOA progressive failure analysis. This step serves to evaluate the degree of damage caused by the fire. Due to lack of degradation data of composite material properties with respect to temperature, a Multi-Factor Interaction Model (MFIM) is utilized to estimate degradation. The MFIM describes the Material Behavior Space (MBS) as an n-dimensional space. The progressive sub-structuring of MFIM leads to a multi-tier representation of the MBS, which permits intrinsic lower tier behaviors to influence more than one factor at the next higher tier. This representation is computationally efficient and represents a general trend and not the entire precise path from its reference value to its final value. The results

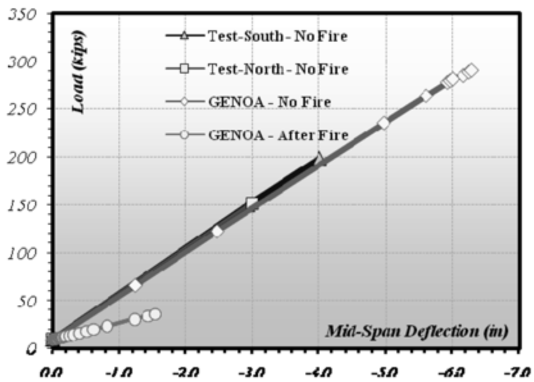

Fig. 6 Comparison of load displacement curves before and after fire exposure

indicate that fire damage was mainly distributed on the top deck and the vast majority of damage was attributable to failure associated with the Modified Distortion Energy (MDE) Criterion (Chamis 1969).

Returning to the analysis, the damage index, at the second stage, is imported to the third stage to continue structural progressive failure analysis with respect to the defined structural load. Progressive Failure Analysis continues until the last equilibrium point is found, which corresponds to ultimate failure. The load displacement curves for the original and damaged bridge are shown in Fig. 6. From this figure, it is obvious that fire has a severe effect not only on the stiffness of whole structure but also on the failure load. In previous studies, the failure load on the original CAB without fire was 235 kips (1,045.3 kN). After the fire exposure, it was found to be 36 kips (160.1 kN), which indicates that the residual strength is a mere 15% of the original strength under identical maximum shear loading schemes. It can be concluded that fire will dramatically reduce the stiffness and strength of composite army bridge.

3.6. Application of the mockup beam model

Upon completion of the CAB study, a GENOA model of the mockup beam was developed for design and analysis. This model consists of 4,917 nodes and 6,240 elements, including 2,564 solid elements and 3,676 shell elements. The elements were defined using seven material property sets to account for the different materials and layups used in the beam. Once again, progressive failure analysis is utilized to determine the ultimate static load of the beam when subjected to simple four-point flexure. Analysis indicated that ultimate failure took place at a load of 139.1 kips (617.6 kN). The deflection of the middle bottom of the mockup beam showed a slight nonlinearity, which is due to the increasing local damage of the beam. Fig. 7 shows the history of central deflection and damages on the MCB mockup beam. According to the simulation model, ultimate failure occurred after the last equilibrium at 139.1 kips (617.6 kN).

3.7. Combining components during static and cyclic loading of MCB mockup beams

As part of the continuing development of DPS, a series of tests were performed on the MCB mockup beam that utilized the strain gages and optical fiber strain sensors that had previously been mounted by UCI personnel. These cyclic tests consisted of half-cycle push tests and full reversal cyclic tests. They provided the research effort with the opportunity to evaluate the optical fiber interrogation system and

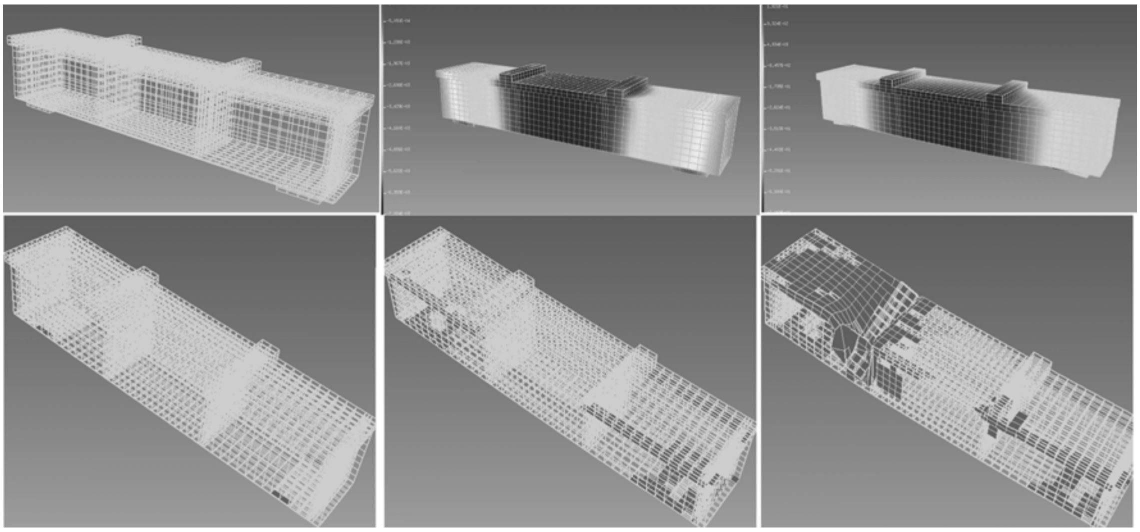

Fig. 7 Progression of central vertical displacement and damage of MCB mockup bridge

capture and compare live strain data from both gages and sensors. Strain data was supplemented by deflection, which was captured using an electronic string potentiometer.

All tests were performed at a low-level loading range (20 kips; 89 kN) in order to avoid any catastrophic damage to the specimen. This loading level was calculated to be 17% of the predicted ultimate load of the MCB mockup specimen. The specimen was subjected to a simply-supported a four-point loading protocol. To avoid stress concentration at the loading and reaction regions, elastomeric pads were placed at the interface between the 2 in (50 mm) high-strength steel rods and the top and bottom chords of the MCB mockup specimens as well as at the interface between the end portions of the bottom chord and the supporting steel fixtures. The loads were transferred using a group of high strength threaded rods and nuts. All tests were undertaken in the steel loading frame using a calibrated ±55 kip (±250 kN) MTS servo-hydraulic actuator with max stroke of ±6 in (±153 mm). The average temperature and relative humidity during the tests was 72ºF (22.2 ºC) and 45%, respectively.

For the first test, the maximum load level was 20 kips (89 kN) with a maximum mid-span deflection of 0.15 in (3.80 mm). As expected, a permanent set did not develop. For the full reversal cyclic loading test, an uneven hysteresis was observed where the maximum mid-span deflection at the push direction was similar to the loading/unloading tests (δ mid-span $\approx$ 0.15 in/3.80 mm), while the corresponding maximum deflection during the pull cycle was 0.34 in (8.6 mm). The uneven behavior was attributed to an unsymmetrical geometry of the cross-section as well as the gap that was observed between the steel rods and the bottom chord. This gap was eliminated in subsequent tests. As shown by the strain vs. time measurements, the optical interrogation system captured data in real time and transmitted it to the CVT in the form of fixed length data packets. In this way, collected strain data was compared to simulated data and previously established failure thresholds.

3.8. Experimental verification

In a series of tests conducted at the University of California at Irvine (UCI), DPS was presented with a real world application involving the four-point bending of a simply supported composite bridge section. The actual specimen was fabricated at Gulfport, Mississippi by Seemann Composites, Inc. To capture the strain data, optical fiber sensors were embedded in the beam during actual fabrication. The beam was 53 inches in length and consisted of a tension rail, four foam bulkheads and a balsa wood core that were all wrapped in a carbon fiber. After the individual components were bonded together, the entire assembly was wrapped in carbon fiber sidewalls. The unit was then shipped to UCI for testing.

The delivered specimen included fourteen optical fiber sensors. Eleven were embedded in the specimen and three were mounted on the surface. The sensors were divided between two optical fiber strands, or cables, that extended about three feet from the body of the specimen. After carefully placing the specimen in the test frame with the appropriate fixturing, the two optical fiber lines were connected to the FSI box for interrogation and data broadcast. The FSI box was in turn connected to a desktop computer by way of an Ethernet connection. Prior to testing and broadcasting, the test operator configured the FSI box to identify the location of the sensors and establish the proper connection protocol with the cellular network and ISP.

Load was applied to the specimen through a 55 kips servo-hydraulic actuator. Although a full suite of automated software supported the actuator, the test program was conducted in manual control with the test operator utilizing both force and displacement control modes to position the actuator head and apply load to the beam. Simultaneous to the preparations in the laboratory, a CVT operator, in another location, loaded a model of the bridge onto the system, specified the sensors to be read, and activated a tool within CVT, which readied the system for the retrieval of live data. Once the actuator head was in position and the CVT was initialized to accept data, the test operator moved to the desktop and commanded the FSI to begin capturing, recording and broadcasting data from the optical fiber sensors. With all data related devices activated, the next task of the test operator was to apply live load to the specimen.

Load was applied in one thousand pound increments from zero to ten thousand pounds. Immediately and in response to this activity, the CVT launched a window that depicted live strain values for each sensor in the form of a dark green curve placed in a chart that plotted strain versus time. A light green curve and a bright red line augmented each chart. The light green curve corresponded to simulated strain for the given location in the bridge and the red curve represented maximum threshold strain generated by simulation for the same physical location. Here, all simulated values were extracted from the GENOA analyses of the FEM model.

Under initial loading, the DPS showed a slight discrepancy between live test data and simulated values. However, once a significant load was applied to the system, i.e. in excess of 3000 pounds, less noise was in the system and the live data and the simulated data showed excellent correlation for all sensors. In this region, the discrepancy between live data and simulated for all three sensors was within ten percent.

In general, simulated data was in good agreement with live data. Since the test did not exceed ten thousand pounds, which is well within the working range of the actuator and the beam, it was assumed that damage did not occur anywhere in the specimen. However, to highlight the warning system associated with DPS, the test operator utilized an interactive feature within the tool that allows a user to adjust the value and location of the red line in terms of percentage of maximum threshold strain. In this way, an operator would be able specify that a warning light should be triggered if a specimen experiences strain that is, for example, sixty percent of the maximum threshold value.

3.9. DPS: structural evaluation of the temporary field repair system

In order to evaluate the effectiveness of a general repair system, three tests were performed on three specimens that were cut from modules of the prototype composite bridge. The dimensions of each specimen were 8 in (0.2 m) by 48 in (1.22 m). The "undamaged" specimen was used as a "control" specimen and was tested to failure in order to determine the ultimate failure load and failure strain, as well as, identify the mode or modes that triggered failure.

The second test was performed on the damaged specimen, whose area of adulteration corresponded to severe damage to the top carbon/epoxy face and severe damage to the balsa core. The objective of the second test was to determine the residual stiffness and strength of the partially damaged specimen as compared to both the undamaged and the repaired specimens. The third test was performed on a repaired specimen that was identically damaged as specimen two but was later repaired using temporary field repair procedures. The repair process consisted of filling the engineered void, i.e. damage, with a two to one mixture of find sand and then bonding a single layer of thin cross-ply cloth over the surface of the specimen, so that the wound is completely covered.

All specimens were tested in a 4-point flexural loading configuration. Two line loads were applied at a distance of 6 in (152.4 mm) from the center of each specimen. The loads were applied in the form of a ramp with a loading rate of 2 kips/min (8.9 kN/min) and were performed up to failure. All specimens were instrumented by both electrical strain and deflection gages. Elastomeric pads were placed at the supports and the line load applications, in order to avoid premature failure due to the expected high stress concentration at these locations. The behavior of the undamaged specimen was linear up to a load level of 13 kips, after which, slight gradual stiffness degradation was observed. As indicated in Fig. 8, the ultimate failure load was 24.13 kips (107.33 kN) with a maximum deflection at the mid-span of 0.57" (14.48 mm) with an initial stiffness of 38 kip/in. The mode of failure was brittle in the form of local debonding, in the unsupported right portion of the specimen between the right support and the line

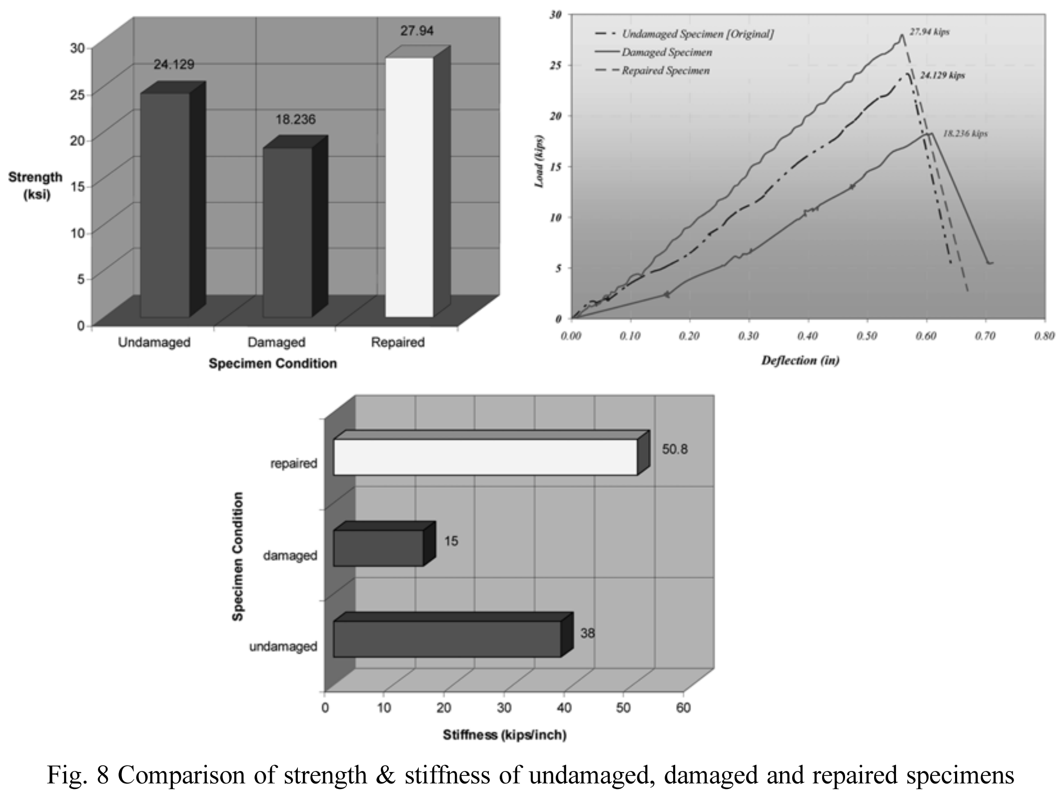

Fig. 8 Comparison of strength & stiffness of undamaged, damaged and repaired specimens

load, followed by a local buckling. Simultaneously, the balsa wood core failed suddenly including the splitter, or intermediate laminate. No failure was observed in either the top or bottom composite face sheet.

The damaged specimen was tested using the same setup as the undamaged specimen. From the start, this specimen showed a lower stiffness as compared to the control specimen with an average initial linear stiffness of about 15 kip/inch. The ultimate load of this specimen was 18.24 kips (81.13 kN) which was about 75% of the ultimate capacity of the undamaged specimen. The corresponding mid-span deflection at the ultimate load was slightly larger than the corresponding deflection of the undamaged specimen (0.61 in (15.5 mm) vs. 0.57 in (14.48 mm)). Unlike the undamaged specimen, the failure was initiated at the pre-damaged area located between the two line loads. This can be attributed to the major reduction of the area and stiffness of the compressed face sheets at the damaged area.

The first mode of failure was a compression failure of one of the two 2 in × 8 in (51 mm × 203 mm) top face sheets at the neighborhood of the right line load. As a result, debonding of the face sheet at the damaged region occurred followed by delamination of this portion of the face sheets, which extended 3" (76 mm) from the line load. At the same time, local damage to the balsa core was observed.

For the repaired specimen, the test setup was, once again, identical to the setup used for both the undamaged (*control*) and the damaged specimen. As compared to the other two specimens, both the initial and the average flexural stiffnesses of the repaired specimen were relatively higher. In general, the behavior was linear up to the failure load that was reached at 27.94 kips (124.3 kN). Thus, the strength of the repaired specimen was 16%, and 53.2% higher than the flexural strength of the undamaged and damaged specimens, respectively. The maximum mid-span deflection at the ultimate load was 0.55 in (13.9 mm) which is slightly smaller that the corresponding deflection of both the undamaged and damaged specimens. The average stiffness of this specimen was 50.8 kip-in, which is 338% of the average stiffness of the damaged specimen and 133% of the original undamaged design. In conclusion, the repair procedures was very effective in not only restoring the original capacity, but also resulted in a 16% increase in the strength of the original design. In addition, the repair procedure upgraded the flexural stiffness more than 3.4 fold as compared to the stiffness of the damaged stiffness. The ultimate failure of this specimen was initiated by debonding of the top balsa core from the intermediated separation laminate. This was followed by localized core failure at different locations.

4. Conclusions

This paper presented the results of an on-going program that is developing novel techniques and a defined methodology to monitor and repair composite bridges. Following the introduction, Section 2 provided background information on progressive failure, GENOA, and diagnostic monitoring of remote structures, which explained how the individual components provided a foundation for DPS. Section 3.1 exposed the DPS to a real world application. In general DPS functioned effectively. Data from the test article was delivered to the CVT and compared to simulation data from a corresponding GENOA model. The two sets of data exhibited good correlation and were not encumbered by delays or other technical challenges. Once system noise was reduced, the average error between the live data set and the simulated data set did not exceed ten percent. Results suggest a full suite of verification examples would be useful when describing and defending the efficacy of the DPS. Further evolution of the tool in terms of redundant data transmission and expanded interactive software is warranted.

The experimental results showed the repaired specimen performed significantly better than the undamaged and damaged specimen in all observed categories. This result called into question the fundamental quality and merits of the original design of the composite chord and by default the composite deck, which, in turn, is a major component of the composite bridge. The findings indicates that the original design of the composite bridge may require further optimization, since the limit-state is *debonding and core strength* rather than the *strength of the composite top face sheet*. It should be noted that the thickness of the repair laminate was more than 10 times less than the thickness of the original face sheets. Despite this reduction the strength and stiffness of the repaired specimen were higher than those of the original approach. Beyond design, it is recommended that further testing with alternative repair procedures should be undertaken. A qualitative assessment of competing rehabilitation methodologies would be a valuable contribution to the repair knowledge base. In addition, the next generation of repairs should utilize DPS by employing intelligent fiber optic patches or traditional embedded fiber optic sensors wherever possible.

References

Abdi, F., Surdenas, J., Mosallam, A. and Wang, J.J. (2003), *Field repair technology for composite bridges*, phase I final report, Submitted to U.S. Army TACOM.

Advanced Composites for Bridge Infrastructure Renewal-Phase II (2000), *DARPA Agreement 0030, Volume II-Task No. MDA972-94-3-14*, Submitted to DARPA by Advanced Composites Technology Transfer/Bridge Infrastructure Renewal Consortium.

Chamis, C.C. (1969), *Failure Criteria for Filamentary Composites, Composite Materials Testing and Design: ASTM STP 460*, (American Society for Testing and Materials).

Chamis, C.C. and Sinclair, J.H. (1979), *Micromechanics of Intraply Hybrid Composites: Elastic and Thermal Properties*, NASA TM-79253.

Hill, R. (1950), *The Mathematical Theory of Plasticity*, Oxford University Press, Oxford.

Morrow, J. (1968), *Fatigue Design Handbook*, Society of Automotive Engineers, Graham.

Mosallam, A.S. and Haroun M.A. (2003), "Tructural evaluation, repair and construction of a composite highway bridge deck", *2nd Int. Workshop on Structural Composites for Infrastructure Applications*, NSF/HBRC, Cairo, Egypt, December 17-18.

Mosallam, A., Ramki, I. and Abdi, F. (2005), *Progressive Failure Analysis of Composite Army Bridge*, CICE Publications, Australia.

Murthy, P.L.N. and Chamis, C.C. (1986), "Integrated composite analyzer (ICAN): users and programmers manual", NASA Technical Paper 2515.

Nakazawa, S., Dias, J.B. and Spiegel, M.S. (1987), *MHOST Users' Manual*, Prepared for NASA Lewis Research Center by MARC Analysis Research Corp.

Ramki, I., Mosallam, A. and Abdi, F. (2004), "Progressive failure analysis of composite army bridge", *The Second Int. Conf. on FRP Composites in Civil Engineering*, Adelaide, Australia, December 8-10.

Tsai, S.W. (1968), *Strength Theories of Filamentary Structures, in Fundamental Aspects of Fiber Reinforced Plastic Composites*, edited by R.T. Schwartz and H.S. Schwartz, Eds., Interscience, New York.